SCICELL

Nova Biotechnol Chim (2020) 19(2): 138-153
DOI: 10.36547/nbc.v19i2.769

Nova Biotechnologica *et* Chimica

Thermodynamics and cooperativeness of the spin crossover

Roman Boča✉

Department of Chemistry, Faculty of Natural Sciences, University of SS Cyril and Methodius in Trnava, Trnava, SK- 917 01, Slovak Republic

Article info

Article history:
Received: 17th July 2020
Accepted: 11th September 2020

Keywords:
Cooperativeness
Spin crossover
Statistical analysis
Thermodynamic parameters

Abstract

Spin transition – a passage from the low-spin electronic state to the high-spin one of Fe(III) and Fe(II) complexes is assessed from several points of view: theoretical modelling, magnetic susceptibility data, and calorimetric measurements. The concept of the cooperativeness in the solid state is discussed in detail. Thermodynamic parameters are mutually correlated for a set of analogous Fe(III) complexes by using modern statistical methods.

Introduction

Thermally driven passage from the low-spin electronic state to the high-spin one is usually termed the spin crossover though also spin transition, spin conversion, and spin equilibrium is frequently used in this content and confused in their meaning. This phenomenon can be considered as a kind of unimolecular reaction where the conversion from L (low-spin) to H (high-spin) states is an process driven by entropy. For such a case $\Delta S > 0$ and $\Delta H \sim k_B T > 0$ hold true so that there exists a critical temperature given by the ratio $T_{1/2} = \Delta H/\Delta S$; above $T_{1/2}$ the change in Gibbs energy alters to $\Delta G < 0$ so that the conversion progresses spontaneously. Thermal development of the high-spin mole fraction x_H can be used in monitoring conversion degree; the equilibrium constant is expressed as $K = x_H/(1 - x_H)$. In an ideal case the ln$K$ *vs* $1/T$ dependence is a straight line (Fig. 1).

The spin conversion is often explained using the orbital diagram, as presented in Fig. 2 for mononuclear Fe(II) and Fe(III) complexes. Electrons promoted from the non-bonding orbitals t_{2g} into the antibonding orbitals e_g cause a softening of the adiabatic potential $E = f(R)$ (force constants k(H) < k(L) with its minimum lying at higher

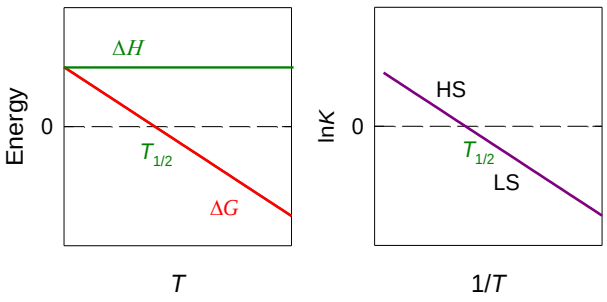

Fig. 1. Schematic representation of the spin crossover as entropy driven unimolecular reaction.

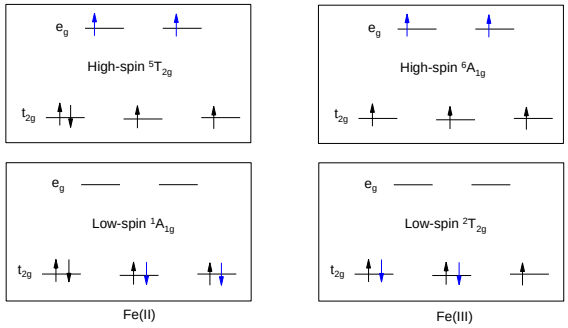

Fig. 2. Orbital diagram showing a difference between the low-spin and high-spin complexes Fe(II) and Fe(III) in an octahedral geometry.

✉ *Corresponding author:* roman.boca@ucm.sk

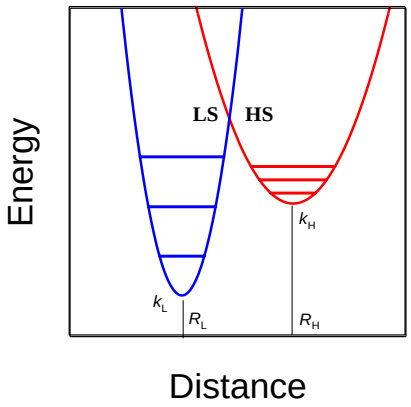

Fig. 3. Interrelation of the adiabatic potentials for the low-spin and high-spin states.

metal-ligand distances, R_0(H) > R_0(L) (Fig. 3).

The electronic contribution to the transition entropy is given by the spin multiplicities as follows $\Delta S_{el} = R\ln[(2S_H+1)/(2S_L+1)]$; this amounts to 9.1 and 13.4 J K^{-1} mol^{-1} for Fe(III) and Fe(II) complexes, respectively. A softer adiabatic potential for the HS state implies denser vibrational energy levels which enhances the vibrational contribution to the transition entropy: S_{vib}(H) > S_{vib}(L).

Generalized crystal field theory

In explaining the spin crossover phenomenon often an orbital picture is utilized. However, this simple approach abstracts from the mutual repulsion of energy and also the spin-orbit coupling. Therefore, there is a need of a more sophisticated approach to the spin crossover by using quantum-chemical calculations. Herein the generalized crystal field theory (GCF) has been applied for such a purpose with numerical outputs (Boča 2006).

The interelectron repulsion is involved by considering the set of atomic terms labelled by the orbital and spin quantum numbers, i.e. $|\alpha, L, S, M_L, M_S\rangle$. A passage to the complex belonging to a point group **G** requires considering a set of crystal-field (CF) terms $|\alpha, \Gamma, \gamma, S, M_S\rangle$ (like $^2T_{2g}$, $^6A_{1g}$, etc.) where g is the component of the multidimensional irreducible representation G. The spin-orbit interaction (SOI) splits the CF-terms into a set of crystal-field multiplets $|\alpha, \Gamma', \gamma'\rangle$; they need be classified using the irreducible representations of the respective double group (Γ_1 through Γ_8 for **O'** in Bethe notation).

In terms of the GCF, a theoretical modelling has been done for Fe(III) [and Fe(II)] systems by involving the interelectron repulsion *via* Racah parameters B = 1,122 [897] cm^{-1} and C = 4.2 B, crystal-field poles for individual ligands F_4(L), spin orbit interaction with the coupling constant ξ = 460 [400] cm^{-1}, orbital-Zeeman and spin-Zeeman interactions (Boča and Herchel 2015). The overall interaction matrix (Eq. 1):

$$\{V^{ee}(B,C)+V^{cf}(F_4)+V^{soi}(\xi)+V^{oZ}(B)+V^{sZ}(B)\} \xrightarrow{\text{diagonalization}} E_i(B) \quad (1)$$

is diagonalized and the calculated Zeeman levels $E_i(B)$ form the partition function (Eq. 2):

$$Z(B,T) = \sum_i \exp[E_i(B)/k_B T] \quad (2)$$

Finally, the formulae of the statistical thermodynamics can be utilized in order to calculate magnetization and magnetic susceptibility (Eq. 3 and 4):

$$M_{mol}(B,T) = -\left(\frac{\partial F}{\partial B}\right) = RT\left(\frac{\partial \ln Z}{\partial B}\right)_T \quad (3)$$

$$\chi_{mol}(T) = \mu_0\left(\frac{\partial M_{mol}(B,T)}{\partial B}\right)_{B_0} \quad (4)$$

Since the mapping of $E_i(B_k)$ proceeds for discrete field values B_k, numerical derivatives are required that, in fact, are provided after a parabolic fit (Eq. 5).

$$Z(B_k;T_m) = c^{(0)}_{k,m} + c^{(1)}_{k,m}\Delta B_k + c^{(2)}_{k,m}\Delta B_k^2 \quad (5)$$

Effective magnetic moment constructed from the magnetic susceptibility displays a thermal development that strongly depends upon the crystal field strengths – see Fig. 4 for an octahedral Fe(III) system. In a narrow interval of the crystal-field strengths the spin crossover occurs: for the pole strength F_4 = 17,700 cm^{-1}, the ground state is high-spin $^6A_{1g}$ but for F_4 = 18,200 cm^{-1} it is low-spin $^2T_{2g}$.

A delicate situation exists for the intermediate crystal field (Fig. 5): with F_4 = 18,000 cm^{-1} the ground CF-term is high-spin $^6A_{1g}$ so that the spin crossover would not apply. However, the close-lying excited CF-term $^2T_{2g}$(×6) is split due to the spin-orbit interaction by a rather high

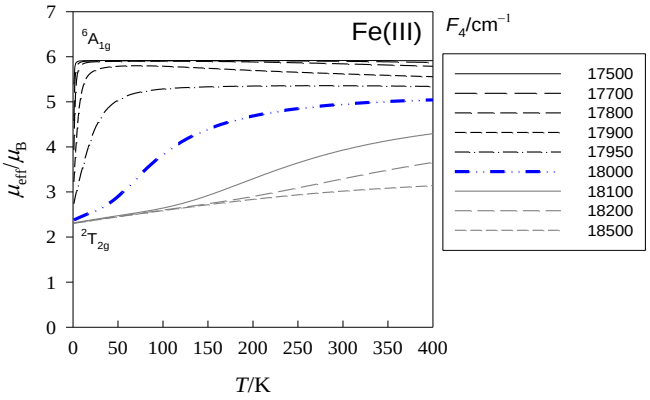

Fig. 4. Calculated temperature evolution of the effective magnetic moment for octahedral Fe(III) systems having various crystal-field strengths $F_4 = 6(Dq)$.

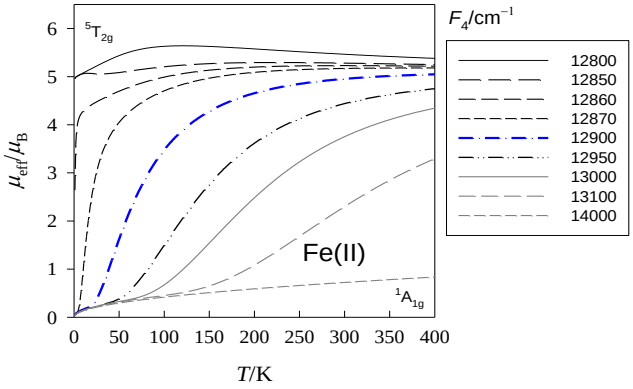

Fig. 6. Calculated temperature evolution of the effective magnetic moment for octahedral Fe(II) complexes having various crystal-field strengths $F_4 = 6(Dq)$.

amount (Δ_{SOI} = 690 cm^{-1}) that overcomes the inter-term gap (Δ_0 = 425 cm^{-1}). Consequently, the ground crystal-field multiplet is the component $\Gamma_7(\times 2) \leftarrow {}^2T_{2g}$ that it is doubly degenerate: $g(\Gamma_7) = 2$. Thus, the change of the electronic entropy (Eq. 6):

$$\Delta S = R\ln[g(A_{1g})/g(\Gamma_7)] = R\ln[6/2] > 0 \qquad (6)$$

is positive so that the spin crossover develops according to the bold curve drawn in Fig. 4.

For Fe(II) systems the situation is different in several aspects (Fig. 6). With a weaker crystal field strength F_4 = 12,800 cm^{-1} ($10Dq$ = 7,680 cm^{-1}), the effective magnetic moment corresponds to the high-spin state with a typical course passing through a round maximum on heating. With a bit higher crystal field of F_4 = 12,870 cm^{-1}, the ground state is low-spin and on heating the effective magnetic moment increases from zero to the value $\mu_{eff} \sim 5.0\ \mu_B$ at the room temperature. A typical spin-crossover behaviour proceeds at F_4 = 12,900 cm^{-1}. For F_4 = 13,000 cm^{-1} the spin conversion is apparently incomplete (it continues to the completeness at the much higher temperature). With F_4 = 14,000 cm^{-1} t he spin transition occurs far above the room temperature and only a "temperature-independent paramagnetism" is visible until T = 400 K.

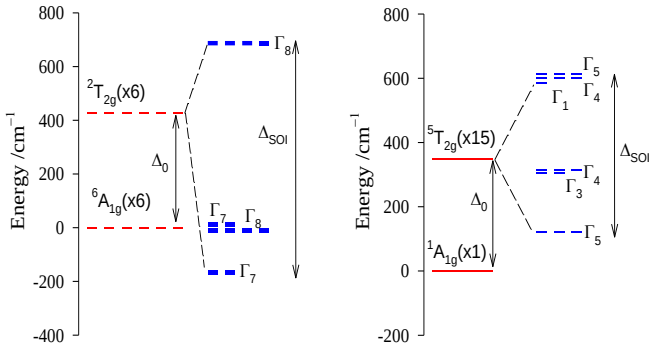

Fig. 5. Left – energies of the lowest crystal-field terms and crystal-field multiplets for F_4 = 18,000 cm^{-1} in Fe(III); right – for F_4 = 12,900 cm^{-1} in Fe(II); calculations involve SOI.

The excited crystal-field term $^5T_{2g}$ is split due to the spin-orbit interaction into three groups of the crystal-field multiplets Γ_5, $\{\Gamma_3 + \Gamma_4\}$ and $\{\Gamma_1 + \Gamma_4 + \Gamma_5\}$. This means that four groups of energy levels are involved in the spin crossover of an octahedral Fe(II) system (Fig. 6).

In octahedral systems the electron repulsion and the crystal field strength are interrelated by the Tanabe-Sugano (TS) diagrams where the term energy (not involving SOI) is plotted versus Dq/B parameter ($\Delta = 10Dq = (10/6)F_4$) – Fig. 7. These diagrams are helpful in identifying the critical ratio when the high-spin complex turns to the low-spin one.

For Fe(II) systems, the crossover of the terms $^5T_{2g} \leftrightarrow {}^1A_{1g}$ exists at the ratio Dq/B = 2.38; this implies Dq = 2,135 cm^{-1} and F_4 = 12,809 cm^{-1}. The last value matches the "observed" on-set of the spin transition. Analogously for Fe(III), the crossover $^6A_{1g} \leftrightarrow {}^2T_{2g}$ appears at Dq/B = 2.70 giving rise Dq = 3,029 cm^{-1} and F_4 = 18,176 cm^{-1}; this again matches the region in which the spin crossover is observed.

The octahedral geometry, however, is rather hypothetical for real spin crossover systems and at least tetragonal and/or trigonal distortions would be more close to the reality. A two-dimensional map of the lowest crystal field terms is presented in Fig. 8 and it can be considered as a generalized

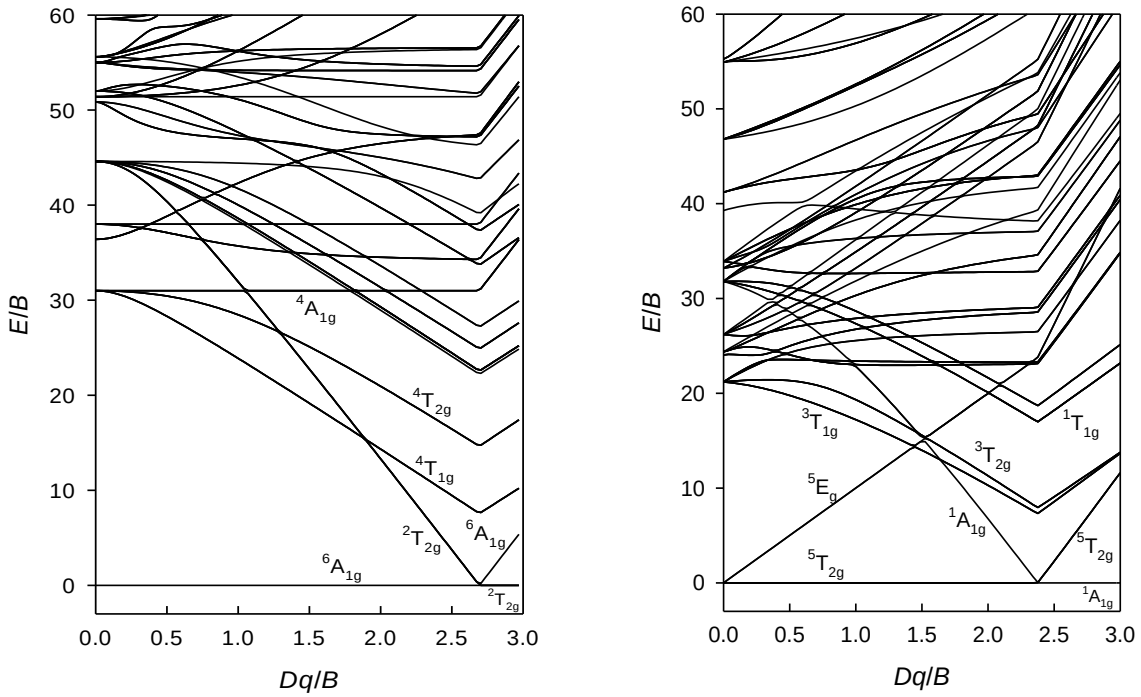

Fig. 7. Tanabe-Sugano diagrams for octahedral Fe(III) and Fe(II) complexes (experimental *B* and *C* parameters were used in calculations).

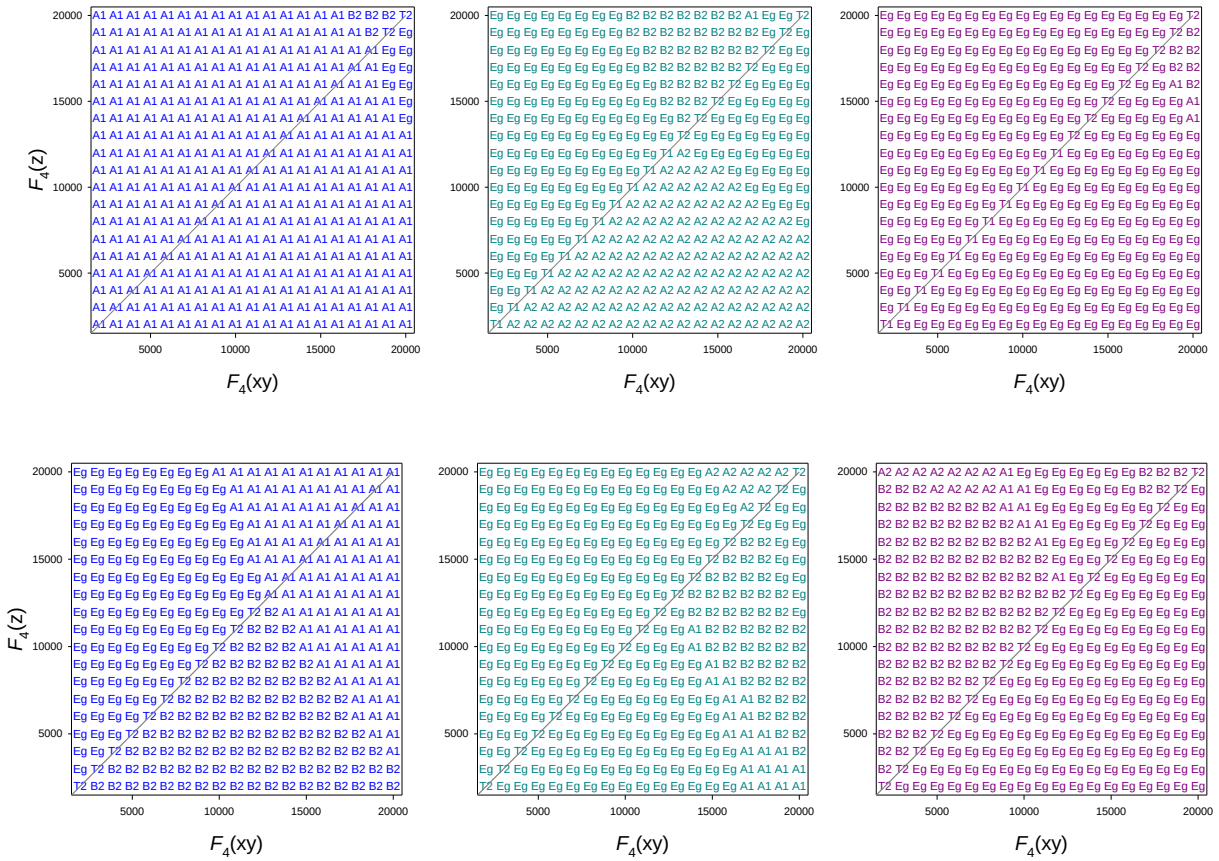

Fig. 8. Generalized Tanabe-Sugano diagrams showing three lowest energy levels for $[FeL_4^{equ}L_2^{ax}]$ bipyramidal complex: top – d^6, bottom – d^5 system; left panel – ground state, centre (right) – first (second) excited state or a component of the degenerate state. Solid line passes through the octahedral arrangement and separates the elongated and compressed tetragonal bipyramid.

TS-diagram (SOI not involved) allowing a bordering of the spin crossover. When the pole strengths $F_4(z) = F_4(xy)$, the diagram collapses to the TS one.

In the TS diagram the crossover point refers to a situation when the LS and the HS state are accidentally degenerate. According to Fig. 3, the metal-ligand distances obey $r_L < r_H$. In Fe(II) complexes, these typically are r_L ~1.96 - 2.00 Å and $\Delta r_{HL} = r_H - r_L$ ~ 0.16 - 0.21 Å. This shift manifest itself into the ligand field strengths owing to the relationship $R = (10Dq^L/10Dq^H) = (r_H/r_L)^5$. This ratio amounts to $R \sim (2.2/2.0)^5 = 1.6$ so that on passing from HS to LS, the ligand strength increases approximately by a factor of 2 and vice versa. In the TS diagram of iron(II) spin crossover compounds $10Dq^H$ will be situated at the left and $10Dq^L$ to the right of the crossover point.

It must be emphasized that the above modelling refers to electronic factors only and they completely ignore the important contribution of the molecular vibrations to the spin crossover. Also, vertical excitations in electronic transitions are assumed instead of the adiabatic ones.

The spin crossover can appear also for Mn(III) systems ($S_L = 0$ to $S_H = 2$ transition) as well as Co(II) complexes ($S_L = 1/2$ to $S_H = 3/2$ crossover).

Master equation

For description of the spin crossover, a number of different theoretical models have been developed so far (Wajnflasz 1970; Bari and Sivardiére 1972; Slitcher and Drickamer 1972; Sorai and Seki 1974; Zimmermann and König 1977; Rao *et al.* 1981; Spiering *et al.* 1982; Adler *et al.* 1987; Bousseksou *et al.* 1995; Cantin *et al.* 1999; Boča *et al.* 2003). Their attempt is to simulate a development of the high-spin mole fraction x_H under the thermal propagation: $x_H = f(T)$. One of these models is the *regular solution & domain model* based upon general principles of thermodynamics.

The first step in the regular solution model is consideration of mixing entropy S_{mix}; this results from the distribution of the LS and HS molecules within the system of N molecules that is simplified by exploiting the Stirling formula for factorials (Eq. 7):

$$S_{mix} = k_B \ln \frac{N!}{(xN)![(1-x)N]!} = -k_B N\{x \ln x + (1-x)\ln(1-x)\} \quad (7)$$

Here, we utilized that xN molecules are in the HS state and $(1 - x)N$ in the LS one.

Let us consider domains of like spin and of uniform size. Then the number of molecules per domain is $n = N/D$ and the mixing entropy alters to (Eq. 8):

$$S_{mix} = k_B \ln \frac{D!}{(xD)![(1-x)D]!} = -k_B D\{x \ln x + (1-x)\ln(1-x)\} \quad (8)$$

The molar mixing entropy becomes expressed as follows (Eq. 9):

$$S_{mix} = -(R/n)\{x \ln x + (1-x)\ln(1-x)\} \quad (9)$$

where $R = N_A k_B$ is the ideal gas constant.

The second contribution in the play is intermolecular interactions with energy E_{int} constituted as follows (Eq. 10):

$$E_{int} = E_{HH}x^2 + 2E_{LH}x(1-x) + E_{LL}(1-x)^2 = J_0 + J_1 x + J_2 x^2 \quad (10)$$

where E_{HH}, E_{LH}, E_{LL} are the interaction energies between HS-HS, LS-HS and LS-LS pairs, respectively. To this end, a rearrangement offers (Eq. 11):

$$\left.\begin{aligned} J_0 &= E_{LL} \\ J_1 &= 2(E_{LH} - E_{LL}) \\ J_2 &= E_{LL} + E_{HH} - 2E_{LH} \end{aligned}\right\} \quad (11)$$

The molar Gibbs energy adopts the form (Eq. 12):

$$G_x = xG_H + (1-x)G_L - TS_{mix} + E_{int} \quad (12)$$

where G_L and G_H refer to the molar Gibbs energies for the LS and HS units, respectively.

The equilibrium condition requires (Eq. 13):

$$\left(\frac{\partial G_x}{\partial x}\right)_{T,p} = G_H - G_L + (R/n)T\ln\left(\frac{x}{1-x}\right) + J_1 + 2J_2 x = 0 \quad (13)$$

which yields the equation for the mole fraction of the high-spin species (Eq. 14):

$$x = \left\{1 + \exp\left[n(\Delta H - T\Delta S + J_1 + 2J_2 x)/RT\right]\right\}^{-1} \quad (14)$$

An alternative expression is (Eq. 15):

$$x = 1/[1 + f(x)] \quad (15)$$

with the factor (Eq. 16):

$$f(x) = \exp\{[(\Delta H + J_1) - T\Delta S + 2J_2 x]n / RT\} \quad (16)$$

Such an implicit equation requires solution by an iterative procedure.

The entropic term contains two contributions: electronic and vibrational (Eq. 17). The partition function of a set of $m = 3N - 6$ harmonic oscillators ($m = 15$ for a hexacoordinate complex) is

$$z_{\text{vib,L}} = \prod_{i=1}^{m} \frac{\exp(-h\nu_{\text{L},i} / 2k_{\text{B}}T)}{1 - \exp(-h\nu_{\text{L},i} / k_{\text{B}}T)} = \exp\left[\sum_{i=1}^{m} (h\nu_{\text{L},i} / 2k_{\text{B}}T)\right] \prod_{i=1}^{m} \frac{1}{1 - \exp(-h\nu_{\text{L},i} / k_{\text{B}}T)} \quad (17)$$

and analogously for the HS state. Then, in the approximation of an averaged (Einstein) modes $h\bar{\nu}_{\text{L}}$ and $h\bar{\nu}_{\text{H}}$ the entropic term becomes (Eq. 18):

$$\Delta S = \Delta S_{\text{el}} + \Delta S_{\text{vib}} = R \ln\left(\frac{Z_{\text{el,H}} z_{\text{vib,H}}}{Z_{\text{el,L}} z_{\text{vib,L}}}\right) = R \ln\left\{\frac{2S_{\text{H}} + 1}{2S_{\text{L}} + 1}\left[\frac{1 - \exp(h\bar{\nu}_{\text{L}} / k_{\text{B}}T)}{1 - \exp(h\bar{\nu}_{\text{H}} / k_{\text{B}}T)}\right]^m\right\} \quad (18)$$

and the enthalpic one is (Eq. 19):

$$\Delta H = \Delta E_0 + m(h\bar{\nu}_{\text{HS}} - h\bar{\nu}_{\text{LS}})/2 \quad (19)$$

Now the Eqs. 15 – 16 need be solved by an iterative process starting with a trial set of parameters n, $\Delta H + J_1$, $h\bar{\nu}_{\text{L}}$, $h\bar{\nu}_{\text{H}}$ and J_2 for each temperature point. Finally, the equilibrium constant is expressed as (Eq. 20):

$$\ln K = \ln\frac{x_{\text{H}}}{1 - x_{\text{H}}} = -[(\Delta H + J_1) - T\Delta S + 2J_2 x_{\text{H}}]n / RT \quad (20)$$

The effect of the individual parameters to the conversion curve and/or equilibrium constant is presented in Fig. 9.

The condition for the equilibrium (Eq. 13), defines the transition temperature $T_{1/2}$ at which the high-spin and low-spin mole fractions are equal, or $x_{\text{H}} = 0.5$ (Eq. 21):

$$G_{\text{H}} - G_{\text{L}} + J_1 + J_2 = 0\big|_{T=T_{1/2}} = 0 \quad (21)$$

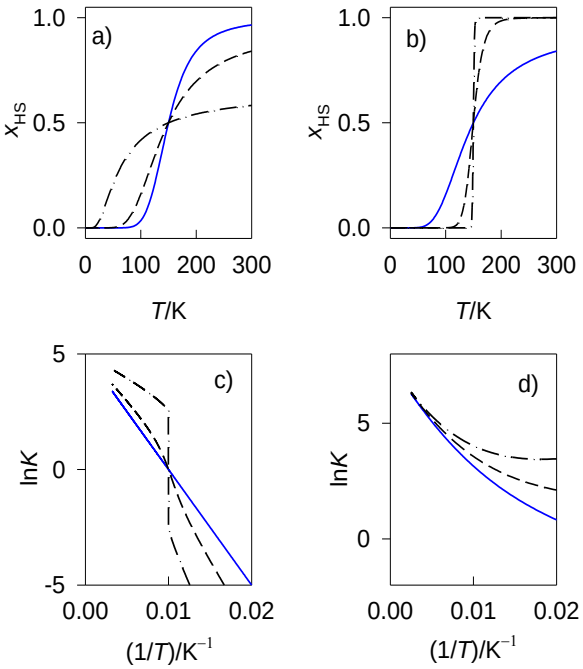

Fig. 9. Conversion curves modelled by the master equation: a) change of the enthalpy $\Delta H/R$ = 100 K (short dashed), 500 K (long dashed) and 1000 K (solid) for fixed $T_{1/2}$ = $\Delta H/\Delta S$ = 150 K and J = 0; b) effect of the domain size n = 1 (solid), 5 (long dashed), 50 (short dashed) for fixed ΔH/R = 500 K and $T_{1/2}$ = 150 K – steepness of the transition; c) effect of the solid-state cooperativeness J/R = 0 (solid), 100 K (long dashed), 300 K (short dashed) for fixed ΔH/R = 500 K and ΔS/R = 5 – deviations from the linearity in the van't Hoff plot; d) effect of molecular vibrations $h\bar{\nu}_{\text{HS}} / k_{\text{B}}$ = 140 K (solid), 160 K (dashed), 180 K (dot-dashed) for fixed $\bar{\nu}_{\text{LS}} = 1.5\bar{\nu}_{\text{HS}}$, $g^{\text{e}}_{\text{HS}} / g^{\text{e}}_{\text{LS}} = 5$, and Δ_0/k_{B} = 600 K.

The transition temperature (Eq. 22):

$$T_{1/2} = (\Delta H + J_1 + J_2)/\Delta S \quad (22)$$

includes also two cooperativity factors; a cancellation of $W = J_1 + J_2$ can be assumed in the theoretical model. One can overcome the two-body interactions (Koudriavtsev 1999) by considering there-body ones producing a third-order term $J_3 x_{\text{H}}^3$ in Eq. 10; this yields an additional term $\Delta T_{1/2} = (3/4)J_3/\Delta S$ in Eq. 22.

Cooperativeness

Within the *regular solution model*, the interaction term involves the solid-state cooperativity factor – *cooperativeness* γ through the expression (Eq. 23):

$$E_{\text{int}} = \gamma x(1 - x) \quad (23)$$

This formula originates in the intercentre interaction (Eq. 24):

$$E_{\text{int}} = J_0 + J_1 x + J_2 x^2 = E_{\text{LL}} + 2(E_{\text{LH}} - E_{\text{LL}})x + (E_{\text{LL}} + E_{\text{HH}} - 2E_{\text{LH}})x^2 \quad (24)$$

which yields the relationship valid for the regular solution&domain model (Eq. 25):

$$\frac{\partial E_{\text{int}}}{\partial x} = J_1 + 2J_2 x = (J_1 + J_2) - J_2(1-2x) = W + \gamma(1-2x) \quad (25)$$

The remainder (Eq. 26):

$$W = J_1 + J_2 = E_{\text{HH}} - E_{\text{LL}} \quad (26)$$

can be absorbed into the effective parameter of the site formation, or it is omitted (Eq. 27):

$$\Delta_{\text{eff}} = \Delta H + J_1 + J_2 \quad (27)$$

Then the factor entering the iteration process (Eq. 14) relaxes to (Eq. 28):

$$f(x) = \exp\{[\Delta_{\text{eff}} - T\Delta S + \gamma(1-2x)]n / RT\} \quad (28)$$

Finally, the cooperativeness becomes expressed in the form (Eq. 29):

$$\gamma = -J_2 = 2E_{\text{LH}} - E_{\text{LL}} - E_{\text{HH}} \quad (29)$$

This expresses a tendency for molecules of one type to interact effectively with molecules of the same spin.

Parameter distribution model was outlined because behaviour of the solid-state samples is non-ideal: a reduction of the cooperativeness can be described using a statistical distribution. High cooperativeness leads to the thermal hysteresis a rectangular shape of the hysteresis loop. Observed profile of the conversion curves, however, is often distorted with marked deviations from the rectangular towards angled shape (Boča *et al.* 2001). The parameter distribution model considers the optimum (maximum) cooperativeness J_2 that drops as follows (Eq. 30):

$$J_{2,i} = n_i J_2 \quad (30)$$

where i is the grid point (e.g. 1/100 of the optimum value $n_{\text{opt}} = 1$). To this end the equation (Eq. 31):

$$x_i = 1/[1 + f(x_i)] \quad (31)$$

contains the factor (Eq. 32):

$$f(x_i) = \exp\{[(\Delta H + J_1) - T\Delta S + 2J_{2,i}x]n / RT\} \quad (32)$$

This equation need be solved by an iterative procedure for the trial set of parameters, for selected temperature, and for each mesh point. The iteration procedure starts with $x_i^{(0)\uparrow} = 0$ in the heating direction, and $x_i^{(0)\downarrow} = 1$ on the cooling path. The averaged value is given by the formula (Eq. 33):

$$x_{\text{H}} = \left[\sum_{i=1}^{\text{Mesh}} w_i \cdot x_i\right] / \left[\sum_{i=1}^{\text{Mesh}} w_i\right] \quad (33)$$

using the weights obeying the Gaussian distribution (Eq. 34):

$$w_i = \exp[-(n_i - n_{\text{opt}})^2 / \delta] \quad (34)$$

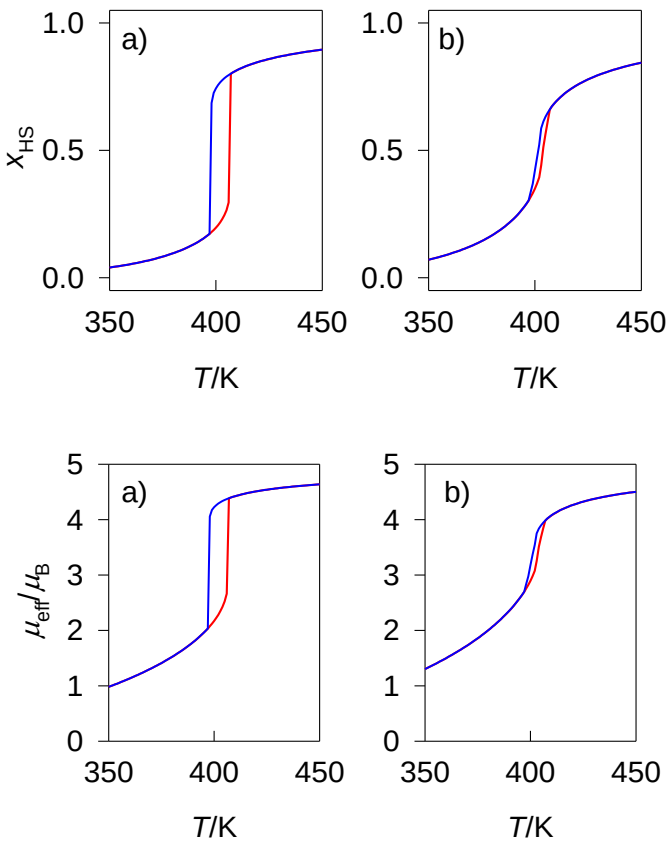

Fig. 10. Parameter distribution model of the spin crossover. Distribution model width: d = 0.00001 (abrupt step) and 0.1 (gradual step). Used parameters: D_0/k_{B} = 2144 K, J/k_{B} = 452 K, r_{eff} = 205 and g_{H} = 2.0. Modelled using the program MIF&FIT (Boča 2016).

The width of the distribution δ leads to the following effects (Fig. 10):

1) $\delta \approx 0$ causes a sharp distribution so that the model collapses to the abrupt step on heating and cooling, respectively. The conversion curve displays a hysteresis loop possessing the rectangular walls.
2) Increased *d* causes that the hysteresis loop has angled walls and a decreased width.
3) With increasing *d* the conversion curve is less complete and visibly smoother.

Thermal hysteresis originates in existence of two minima of the Gibbs energy at different temperatures so that on the heating/cooling the system falls into one of them.

Cooperativeness as the chemical/physical hardness

Let us reconsider pair-wise interactions among solid-state particles (Eq. 35):

$$E_{\text{int}}(x_{\text{H}}) = E_{\text{LL}}(1-x_{\text{H}})^2 + 2E_{\text{LH}}x_{\text{H}}(1-x_{\text{H}}) + E_{\text{HH}}x_{\text{H}}^2 \quad (35)$$

which can be rearranged into the form of a Taylor expansion (Eq. 36):

$$E_{\text{int}}(x_{\text{H}}) = J_0 + J_1 x_{\text{H}} + J_2 x_{\text{H}}^2 \quad (36)$$

The coefficients of the Taylor series are Eq. 37 – 39 (see Fig. 11):

$$J_0 = E_{\text{LL}} \quad (37)$$

$$J_1 = 2E_{\text{LH}} - 2E_{\text{LL}} = \left(\frac{\partial E_{\text{int}}}{\partial x_{\text{H}}}\right) = \mu > 0 \quad (38)$$

$$J_2 = E_{\text{LL}} + E_{\text{HH}} - 2E_{\text{LH}} = \frac{1}{2}\left(\frac{\partial^2 E_{\text{int}}}{\partial x_{\text{H}}^2}\right) = \eta < 0 \quad (39)$$

where *m* – the *chemical potential* that equals to minus absolute electronegativity (Sen and Jorgensen 1987); η – the Pearson's *chemical hardness* (Sen 1993; Pearson 2005).

The cooperativeness *J* is then expressed through an excess of the interaction energy (Eq. 40):

$$J = -J_2/2 = E_{\text{LH}} - (E_{\text{HH}} + E_{\text{LL}})/2 > 0 \quad (40)$$

so that it interrelates to the chemical hardness. Another cooperative contribution is (Eq. 41):

$$W = J_1 + J_2 = E_{\text{HH}} - E_{\text{LL}} \to 0 \quad (41)$$

and it eventually can be neglected.

Recall some additional definitions according to Pearson (Pearson 2005).

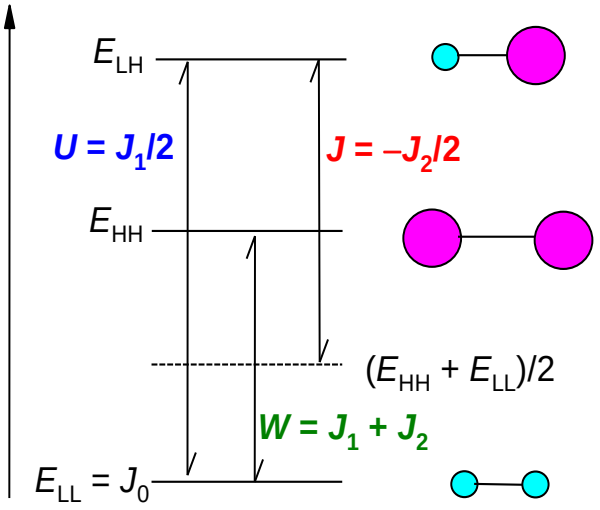

Fig. 11. Interrelations of the interaction parameters.

a) Electronic chemical potential (Eq. 42) – derivative of the energy with the number of electrons at the constant potential generated by a system of nuclei:

$$\mu = \left(\frac{\partial E}{\partial N}\right) \quad (42)$$

b) Absolute electronegativity expressed (Eq. 43) as an average of the ionization energy E_{i} and electron affinity E_{eg}:

$$\chi = -\mu \approx \frac{E_{\text{i}} + E_{\text{eg}}}{2} \quad (43)$$

c) Chemical hardness (Eq. 44):

$$\eta = \frac{1}{2}\left(\frac{\partial^2 E}{\partial N^2}\right), \quad \eta \approx \frac{E_{\text{i}} - E_{\text{eg}}}{2} \quad (44)$$

d) Electronegativity shift for two reactants owing to a transfer of ΔN electrons from 2 to 1 (Eq. 45 and 46):

$$\mu_1 = \mu_1^{\text{o}} + 2\eta_1 \cdot \Delta N \quad (45)$$

$$\mu_2 = \mu_2^{\text{o}} - 2\eta_2 \cdot \Delta N \quad (46)$$

d) Electronegativity (chemical potential) equalization $\mu_1 = \mu_2$ yields (Eq. 47):

$$\Delta N = \frac{1}{2}\frac{\chi_1^{\text{o}} - \chi_2^{\text{o}}}{(\eta_1 + \eta_2)} \quad (47)$$

Electrons move from the site of lower electronegativity to the site of higher electronegativity (Eq. 48). This causes an energy lowering:

$$\Delta E = -\frac{1}{4}\frac{\chi_1^{\circ} - \chi_2^{\circ}}{(\eta_1 + \eta_2)} \quad (48)$$

e) Bulk modulus B and compressibility κ of a solid is (Eq. 49):

$$\frac{1}{\kappa} = B = -V\left(\frac{\partial p}{\partial V}\right)_T, \quad [\text{Pa}] \quad (49)$$

f) *Physical hardness* becomes (Eq. 50):

$$\left(\frac{\partial \mu}{\partial N}\right)_{T,V} = \frac{V}{N^2\kappa} = BV_0 = H, \, [\text{J mol}^{-1}] \quad (50)$$

where V_0 – molar volume, N – number of particles.

g) Fluctuations in the number of particles for a grand canonical ensemble (Eq. 51):

$$\left(\frac{\partial N}{\partial \mu}\right)_{T,V} = \frac{N^2\kappa}{V} = \frac{1}{kT}\left\langle (N - \langle N \rangle)^2 \right\rangle = \frac{\kappa}{V_0} = \frac{1}{H} \quad (51)$$

An ensemble can be crystals of identical volume but with varying numbers of component atoms, i.e. crystals which are physically soft (inverse of hard) possess large fluctuations in N. This set of equations represents a good starting point for investigation of the physical and chemical nature of the solid-state cooperativeness.

Calorimetry *vs.* magnetometry

The classical thermodynamics deals with the volume work $\mathrm{d}w = -p\mathrm{d}V$ and defines two heat capacities (Eq. 52 and 53):

$$C_V = \left(\frac{\partial U(S,V)}{\partial T}\right)_V = R\frac{\partial}{\partial T}\left[T^2\left(\frac{\partial \ln Z}{\partial T}\right)_V\right]_V \quad (52)$$

$$C_p = \left(\frac{\partial E(S,p)}{\partial T}\right)_p = R\frac{\partial}{\partial T}\left[T^2\left(\frac{\partial \ln Z}{\partial T}\right)_V + T\left(\frac{\partial \ln Z}{\partial \ln V}\right)_T\right]_p \quad (53)$$

where Z is the partition function. In the case of the magnetic work $\mathrm{d}w = \mu_0 H\mathrm{d}M$ again two kinds of the heat capacities are distinguished (Eq. 54, 55):

$$C_M = \left(\frac{\partial U(S,M)}{\partial T}\right)_M = R\frac{\partial}{\partial T}\left[T^2\left(\frac{\partial \ln Z}{\partial T}\right)_M\right]_M \quad (54)$$

$$C_H = \left(\frac{\partial E(S,H)}{\partial T}\right)_H = R\frac{\partial}{\partial T}\left[T^2\left(\frac{\partial \ln Z}{\partial T}\right)_M + T\left(\frac{\partial \ln Z}{\partial \ln M}\right)_T\right]_H \quad (55)$$

(Here, enthalpy is denoted as E, not to be confused with the magnetic field strength H.) For the solid state, the appropriate formula for the molar excess-heat capacity measured in the zero field is (Eq. 56):

$$C_p^{\text{ex}} \approx C_M = R\frac{\partial}{\partial T}\left[T^2\left(\frac{\partial \ln Z}{\partial T}\right)_M\right]_M \quad (56)$$

This allows a comparison of the experimental heat capacity (measured using adiabatic or differential scanning calorimeters) with that reconstructed by the theoretical model of the spin crossover (e.g. regular solution&domain model). By substituting the partition function (Eq. 57):

$$Z = \frac{S_{\text{L}}(S_{\text{L}}+1)}{[1-\exp(h\bar{\nu}_{\text{L}}/kT)]^m} \times \left\{1 + \frac{S_{\text{H}}(S_{\text{H}}+1)}{S_{\text{L}}(S_{\text{L}}+1)}\left[\frac{1-\exp(h\bar{\nu}_{\text{L}}/kT)}{1-\exp(h\bar{\nu}_{\text{H}}/kT)}\right]^m\right\} \times \left\{\exp\{-[\Delta E_0 + (h\bar{\nu}_{\text{L}} - h\bar{\nu}_{\text{H}})m/2 + (J_1 + J_2) + J_2(2x-1)]/kT\right\} \quad (57)$$

into Eq. 56, explicit expression for the heat capacity along with its FORTRAN code is obtained by exploiting capabilities of the MATHEMATICA package (Wass 1999).

The heat capacity and/or its weighted function then become a combination of the underlying lattice vibration functions (taken as polynomials) and the excess-heat capacity (Eq. 58 and 59):

$$C_p = (1-x_{\text{H}})(a_{\text{L}} + b_{\text{L}}T + c_{\text{L}}T^2 + d_{\text{L}}T^3) + x_{\text{H}}(a_{\text{H}} + b_{\text{H}}T + c_{\text{H}}T^2 + d_{\text{H}}T^3) + C_p^{\text{ex}} \quad (58)$$

$$(C_p/T) = (1-x_{\text{H}})(a_{\text{L}} + b_{\text{L}}T + c_{\text{L}}T^2 + d_{\text{L}}T^3) + x_{\text{H}}(a_{\text{H}} + b_{\text{H}}T + c_{\text{H}}T^2 + d_{\text{H}}T^3) + (C_p^{\text{ex}}/T) \quad (59)$$

where only some polynomial terms need be considered.

Three complexes under the investigation are characterized as follows (Fig. 12). Complex **1** – [Fe(2-*pic*)$_3$]Cl$_2$·MeOH is a non-cooperative system; its thermodynamic data were scanned by the adiabatic calorimetry (Nakamoto *et al.* 2001).

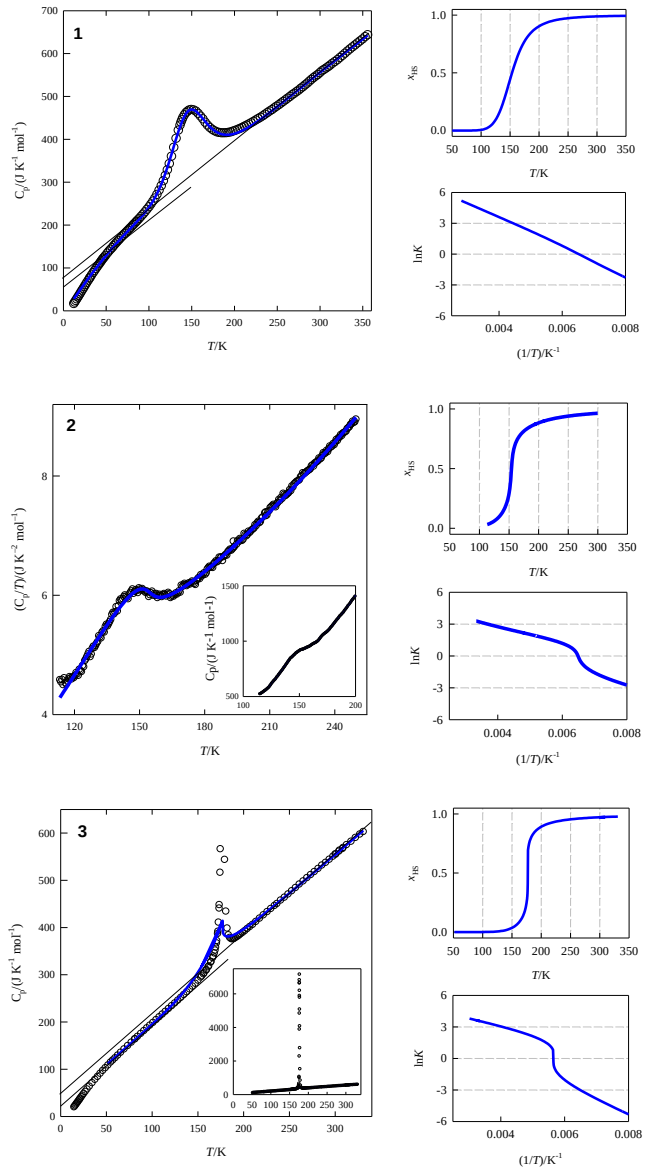

Fig. 12. Experimental (open symbols) and fitted (full lines) thermodynamic functions for **1**, **2**, and **3**.

Complex **2** – [Fe(*pybzim*)$_3$](ClO$_4$)$_2$ belongs to a medium-cooperative system. There is no structural change during the spin crossover as documented by a continuous increase of the lattice parameters. DSC technique has been applied for it (Boča *et al.* 2003).

Complex **3** – [Fe(*phen*)$_2$(NCS)$_2$] is a strongly cooperative system. The effective magnetic moment increases abruptly near the transition temperature $T_{1/2}$ and the structural changes accompany the spin transition.

The thermodynamic data were collected by the adiabatic calorimetry (Sorai and Seki 1974).

The data fitting by the Eq. 56 – 57 gave the set of the spin crossover parameters which are presented in Table 1.

Table 1. Parameters of the spin crossover for complexes **1** through **3** from fitting the heat capacity.[a]

Parameter [b]	Cooperativeness		
	1 – small	**2** – medium	**3** – high
Site format. energy ($\Delta_{\mathrm{eff}}/k_{\mathrm{B}}$) /K	1370	351	1039
Entropic parameters	r_{eff} = 7545	$h\bar{\nu}_{\mathrm{L}}/hc$ = 454 cm^{-1} $h\bar{\nu}_{\mathrm{H}} = h\bar{\nu}_{\mathrm{L}}/1.5$	r_{eff} = 357
Cooperativeness (J/k_{B}) /K	20	136	182
ΔH /kJ mol^{-1}	11.39 [8.88]	2.92 [3.04]	8.64 [8.60]
ΔS /J K^{-1} mol^{-1}	74.2 [59.5]	19.0 [21.0]	48.9 [48.8]
$T_{1/2} = \Delta H / \Delta S$ /K	153 [149]	153 [145]	177 [176]

[a] Values in square brackets are the direct calorimetric determination.

[b] Simplifications: $\Delta S = R \ln r_{\mathrm{eff}}$, $J = -J_2/2$, $\Delta_{\mathrm{eff}} = \Delta E_0 + m(h\bar{\nu}_{\mathrm{L}} - h\bar{\nu}_{\mathrm{H}})/2 + J_1 + J_2$.

Having the experimental heat capacity curve and its temperature-weighted function at the disposal, the numerical integration offers the enthalpy (Eq. 60) and entropy (Eq. 61) of the spin transition:

$$\Delta H = \int_{T_{\mathrm{min}}}^{T_{\mathrm{p}}} C_p' \mathrm{d}T + \int_{T_{\mathrm{p}}}^{T_{\mathrm{max}}} C_p'' \mathrm{d}T \qquad (60)$$

$$\Delta S = \int_{T_{\mathrm{min}}}^{T_{\mathrm{p}}} (C_p/T)' \mathrm{d}T + \int_{T_{\mathrm{p}}}^{T_{\mathrm{max}}} (C_p/T)'' \mathrm{d}T \qquad (61)$$

The measured C_p and C_p/T data need be corrected for the underlying lattice vibrations, for instance, by subtracting polynomial functions applied below T_{min} and/or above T_{max} and the integration limit contains the peak value of T_{p} (Fig. 13).

The integration can be improved by utilizing the conversion curve x_{H} *vs* T known from the measurements of the magnetic susceptibility. This enables a construction of the smooth baseline between C_{min} for the LS and C_{max} for the HS; the excess enthalpy $\Delta H(T)$ (Eq. 62) associated

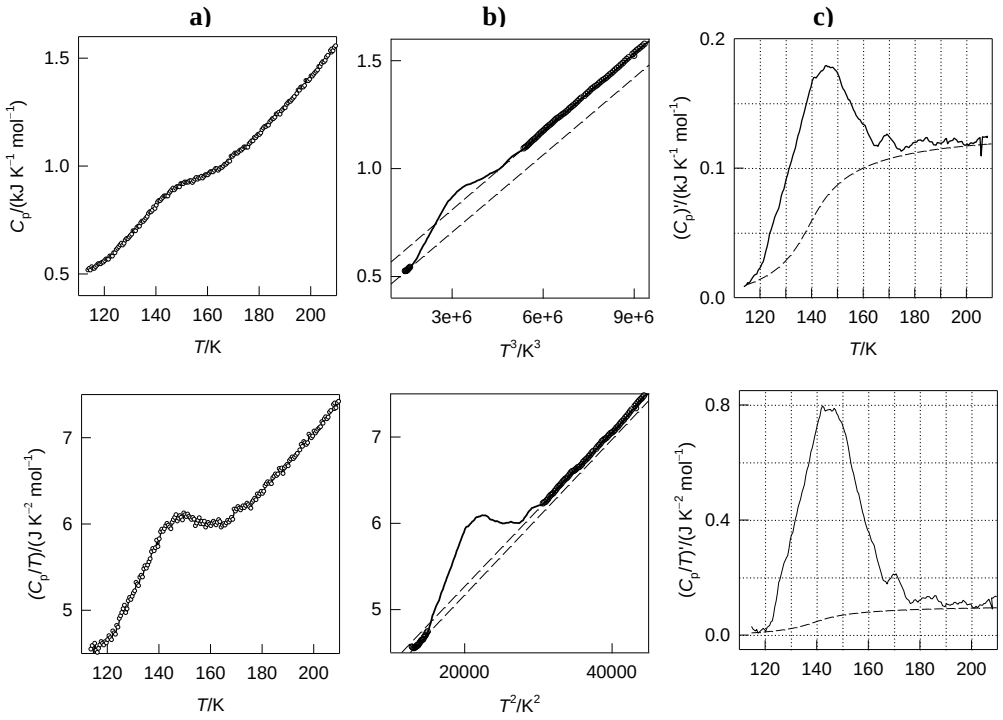

Fig. 13. Heat capacity analysis for [Fe(*pybzim*)$_3$](ClO$_4$)$_2$: **a)** raw data; **b)** data for subtraction of underlying lattice vibrations; **c)** data for numerical integration yielding ΔH and ΔS.

with the spin crossover at the given temperature is:

$$\Delta H(T) = \int_{T_{\min}}^{T} [C_p - (a_{\mathrm{LS}} + b_{\mathrm{LS}} T^3)]\mathrm{d}T - \int_{T_{\min}}^{T} x_{\mathrm{HS}}(C_{\max} - C_{\min})\mathrm{d}T \quad (62)$$

The excess entropy at the given temperature $\Delta S(T)$ can be evaluated in an analogous way.

A direct fitting of the magnetic susceptibility data $\chi(T)$ is possible by considering three contributions in the form of a Curie-Weiss law, namely for the low-spin species, high-spin system, and eventual paramagnetic impurity (Eq. 63, 64, and 65):

$$\chi_{\mathrm{L}} = C_0 g_{\mathrm{L}}^2 S_{\mathrm{L}}(S_{\mathrm{L}}+1)/3(T-\Theta_{\mathrm{L}}) + \alpha_{\mathrm{L}} \quad (63)$$

$$\chi_{\mathrm{H}} = C_0 g_{\mathrm{H}}^2 S_{\mathrm{H}}(S_{\mathrm{H}}+1)/3(T-\Theta_{\mathrm{H}}) + \alpha_{\mathrm{H}} \quad (64)$$

$$\chi_{\mathrm{PI}} = C_0 g_{\mathrm{PI}}^2 S_{\mathrm{PI}}(S_{\mathrm{PI}}+1)/3(T-\Theta_{\mathrm{PI}}) + \alpha_{\mathrm{PI}} \quad (65)$$

where the reduced Curie constant consists of the physical constants, $C_0 = N_{\mathrm{A}}\mu_0\mu_{\mathrm{B}}^2/k_{\mathrm{B}}$. For Fe(II) centres ($S_{\mathrm{L}}$ = 0, S_{H} = 2, S_{PI} = 5/2) the appropriate set of magnetic parameters consists of α_{L}, g_{H}, α_{H}, g_{PI} = 2, Θ_{PI}, and α_{PI}. For Fe(III) centres (S_{L} = 1/2, S_{H} = 5/2) the active set is g_{L}, Θ_{L}, a_{L}, g_{H} = 2.0 and α_{H}. Some of these parameters can be fixed or omitted in order to avoid an overparametrization.

In addition, there are four parameters of the spin crossover that enter evaluation of the conversion curve $x_{\mathrm{H}}(T)$, i.e. Δ_{eff}, J, $h\bar{\nu}_{\mathrm{L}}$ and $h\bar{\nu}_{\mathrm{H}}$ (the last again can be fixed). Then the susceptibility is balanced as follows (Eq. 66):

$$\chi(T) = (1 - x_{\mathrm{H}} - x_{\mathrm{PI}})\chi_{\mathrm{L}} + x_{\mathrm{H}}\chi_{\mathrm{H}} + x_{\mathrm{PI}}\chi_{\mathrm{PI}} \quad (66)$$

and the equilibrium constant (Eq. 67) is:

$$K = x_{\mathrm{H}}/(1 - x_{\mathrm{H}} - x_{\mathrm{PI}}) \quad (67)$$

The enthalpy of the spin transition (Eq. 68) is calculated as a temperature–independent quantity:

$$\Delta H_0 = N_{\mathrm{A}}\Delta_{\mathrm{eff}} = R(\Delta_{\mathrm{eff}}/k_{\mathrm{B}}) \quad (68)$$

which absorbs the site formation energy, zero-point vibration correction, and eventually the cooperativeness parameters (Eq. 69):

$$\Delta_{\mathrm{eff}} = \Delta E_0 + (h\bar{\nu}_{\mathrm{H}} - h\bar{\nu}_{\mathrm{L}})m/2 + (J_1 + J_2) \quad (69)$$

The entropy of the transition (Eq. 70) is a temperature-dependent quantity which at the transition temperature is:

$$(\Delta S)_{T_{1/2}} = R\ln\left\{\frac{2S_{\mathrm{H}}+1}{2S_{\mathrm{L}}+1}\left[\frac{1-\exp(h\bar{\nu}_{\mathrm{L}}/k_{\mathrm{B}}T_{1/2})}{1-\exp(h\bar{\nu}_{\mathrm{H}}/k_{\mathrm{B}}T_{1/2})}\right]^m\right\} \quad (70)$$

This can be approximated through an effective degeneracy ratio (Eq. 71):

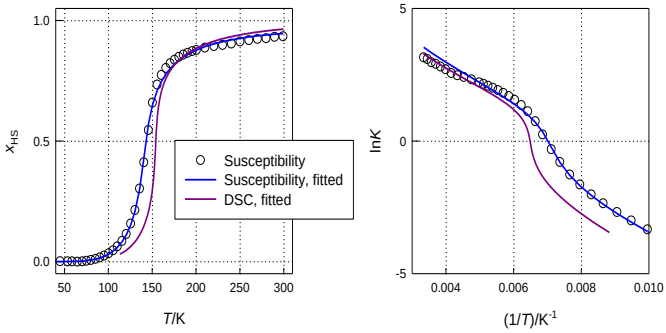

Fig. 14. Comparison of magnetic and calorimetric data for [Fe(*pybzim*)$_3$](ClO$_4$)$_2$. Empty points – experimental data, lines – fitted.

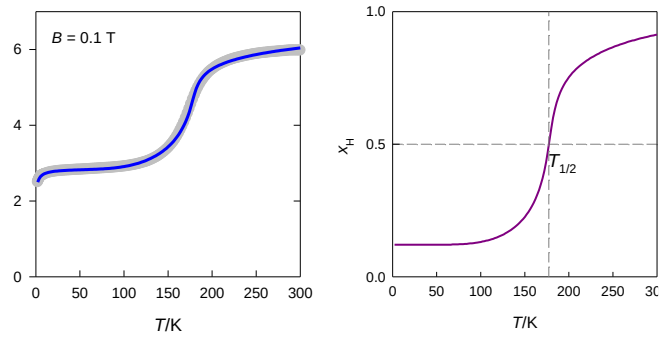

Fig. 16. Magnetic data for [Fe(*napet*)NCS]: left – temperature dependence of the effective magnetic moment, right – a temperature evolution of the calculated high-spin fraction (right); grey circles – experimental data, solid line – fitted.

$$\Delta S = R \ln r_{\text{eff}} \qquad (71)$$

where r_{eff} is subjected to the fitting procedure.
The fitting of the magnetic data and calorimetric data is compared in Fig. 14 on the common basis – temperature evolution of the high-spin mole fraction (left) and the van't Hoff plot (right).

Statistical analysis

A number of organic species H_2L, acting as pentadentate ligands L^{2-}, has been prepared (Fig. 15) by a Schiff condensation between the substituted salicylaldehyde (R-*sal*) and the asymmetric or symmetric triamine (*pet* or *dpt*). Analogously, a set of Schiff-base ligands was obtained using the naphthyl skeleton. They were complexed with Fe(III) salts yielding hexacoordinate [Fe^{III}LX] complexes.
Thermal evolution of the effective magnetic moment showing spin crossover is exemplified in Fig. 16 along with the fitted curve based upon the regular solution model.
In a series of hexacoordinate [Fe^{III}L^{5}X] complexes, the transition temperature $T_{1/2}$ of the spin crossover can be modified by appropriate coligands X (Fig. 17) (Šalitroš *et al.* 2009; Nemec *et al.* 2011; Krüger *et al.* 2013, 2015; Masárová *et al.* 2015). This is affected by the enthalpic and entropic terms since $T_{1/2} = \Delta H/\Delta S$ holds true. It is expected that

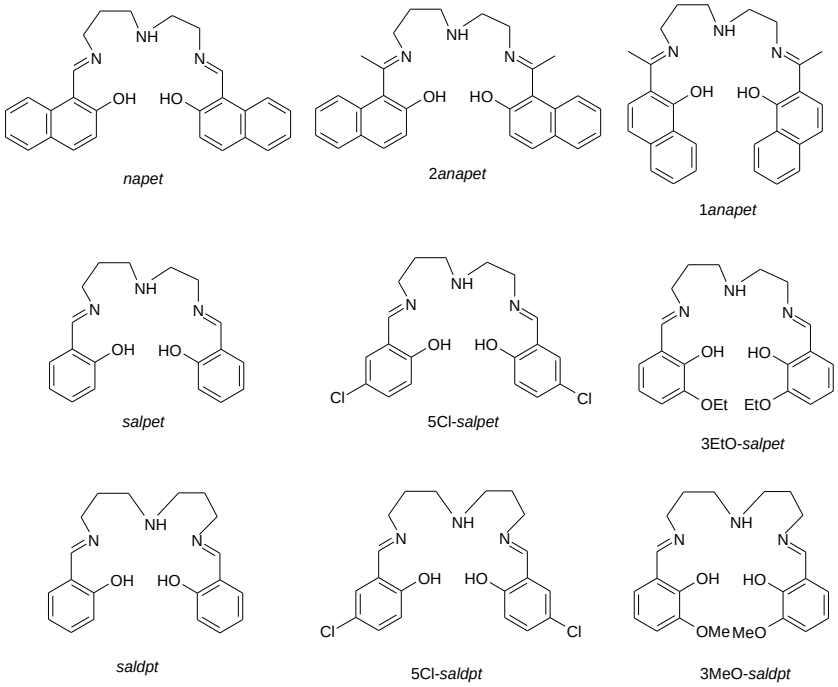

Fig. 15. Sketch of the related pentadentate ligands H_2L^5.

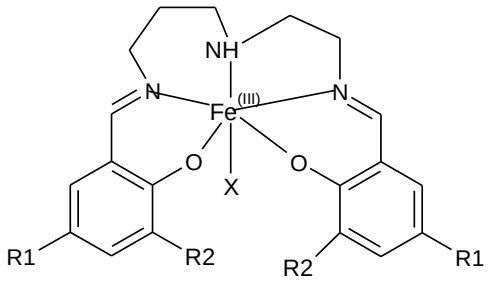

Fig. 17. General form of the [Fe(R-*salpet*)X] type complexes; coligands $X^- = Cl^-$, N_3^-, NCO^-, NCS^-, $NCSe^-$, and CN^-.

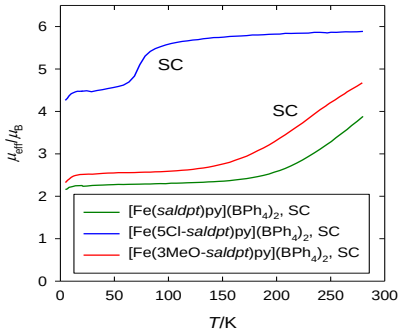

Fig. 19. Spin crossover in complexes of [Fe^{III}(R-*saldpt*)*py*]$(BPh_4)_2$ type.

the value of ΔH can be altered by varying the crystal field strength of involved ligands. However, the factors influencing the value of ΔS are more complex as they include electronic (net spin), vibrational, and other contributions.

Temperature evolution of the effective magnetic moment for related complexes is shown in Fig. 18 and 19. It can be concluded that an increase of the crystal field strength 10*Dq* of the coligand X^- causes a switch of the spin states of complexes from the high-spin state ($X^- = Cl^-$, NCO^-), through the spin crossover ($X^- = NCS^-$, $NCSe^-$), to the low-spin state ($X^- = CN^-$).

In order to unhide latent correlations among thermodynamic parameters influencing the spin crossover, modern multivariate methods were utilized for processing data listed in Table 2: Pearson correlation (PC), cluster analysis (CA) and the principal component analysis (PCA) (Augustín and Boča 2015).

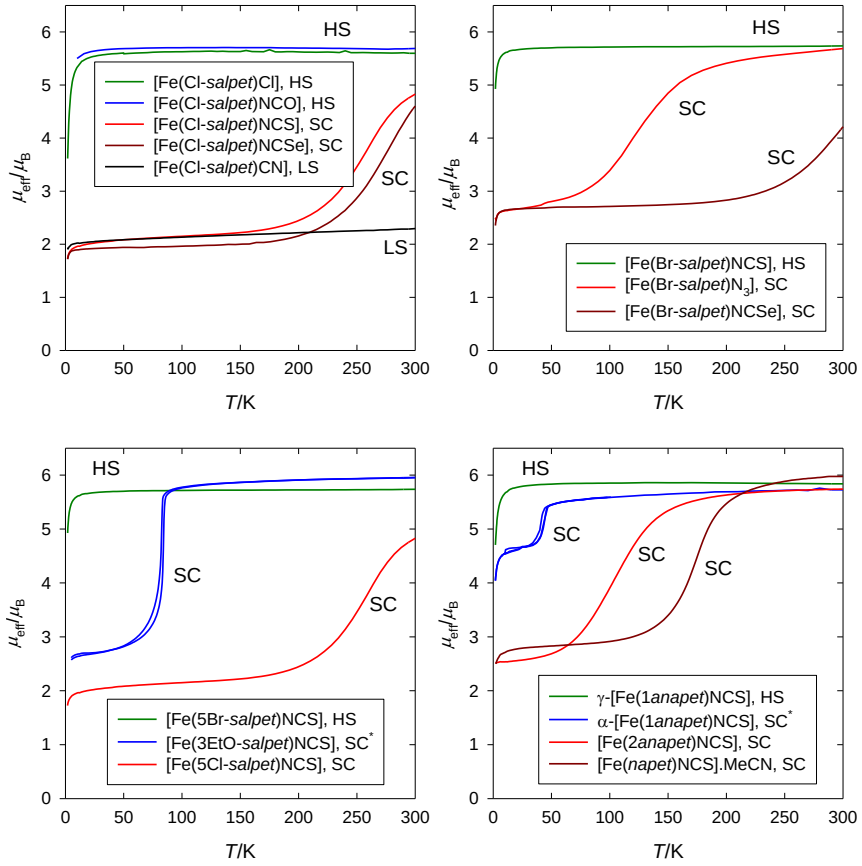

Fig. 18. Comparison of the spin states in complexes of [$Fe^{III}L^5X$] type. Top – fixing the Schiff-base ligand and varying coligand; bottom – varying the Schiff-base ligand and fixing the coligand NCS^-. HS – high spin, SC – spin crossover, LS – low spin. For details consult Table 2.

Table 2. Retrieved thermodynamic parameters for spin crossover systems.[a]

	Compound	$T_{1/2}$	ΔH	ΔS	J
1[h]	[Fe(3EtO-*salpet*)NCS]	84 82	0.9	12	98
2	[Fe(5Br-*salpet*)N_3]·MeOH	142	1.6	11	76
3	[Fe(5Cl-*salpet*)NCS]	280	5.8	21	180
4	[Fe(5Cl-*salpet*)NCSe]	293	6.5	22	197
5	[Fe(5Br-*salpet*)NCSe]	326	6.0	18	215
6	[Fe(*salpet*)*atz*]	416	15	37	284
7[i,h]	α-[Fe(1*anapet*)NCS]	44 40	1.6	4	82
8	[Fe(2*anapet*)NCS]	114	1.6	14	52
9[h]	[Fe(*napet*)N_3]·MeOH	122 117	1.5	11	99
10	[Fe(*napet*)NCS]·MeCN	151	1.9	12	87
11	[Fe(*napet*)NCO]	155	2.5	16	102
12	[Fe(*napet*)NCSe]·MeCN	170	2.3	13	99
13	[Fe(*napet*)NCS]	186	3.3	18	150
14[i]	[Fe(5Cl-*saldpt*)py]BPh_4	78	0.4	6	63
15	[Fe(3MeO-*saldpt*)py]BPh_4	273	4.5	17	90
16	[Fe(*saldpt*)py]BPh_4	310	5.4	17	150

[a] Spin crossover between S = 1/2 and S = 5/2; [h] – spin crossover with hysteresis; [i] – spin crossover between intermediate spin S = 3/2 and S = 5/2. Data of 6 and 7 was omitted in the statistical analysis. Units: $T_{1/2}$/K; ΔH/kJ mol^{-1}; ΔS/J K^{-1} mol^{-1}; (J/k_B)/K. Taken from (Boča *et al.* 2000; Šalitroš *et al.* 2009; Nemec *et al.* 2011; Krüger *et al.* 2013, 2015; Masárová *et al.* 2015).

The results obtained by the cluster analysis are shown in Fig. 20. It can be seen that the complexes under study span two clusters: the cluster 1 is formed by complexes for which below-room temperature spin crossover was observed (No. 1, 2, 8, 9, 10, 12 and 14). The remaining complexes span the cluster No 2 and they show near- or above-room temperature spin transition.

The PCA analysis yields the biplots of principal components shown in Fig. 21. It is seen that the transition temperature $T_{1/2}$ closely relates to the enthalpy and entropy of the spin transition whereas a correlation with cooperativeness J does not exist. The biplot on the right shows the objects spanning into individual clusters which are well separated between two principal components.

Finally, the Pearson correlation evaluates the correlation coefficients for each pair of variables. It is found that $T_{1/2}$ – ΔH pair possesses a high correlation coefficient r = 0.97. As already indicated by CA and PCA analysis, the correlation of the cooperativeness with the remaining parameters is weak. The transition temperature and the transition entropy are plotted *vs* the transition enthalpy along with the regression curve.

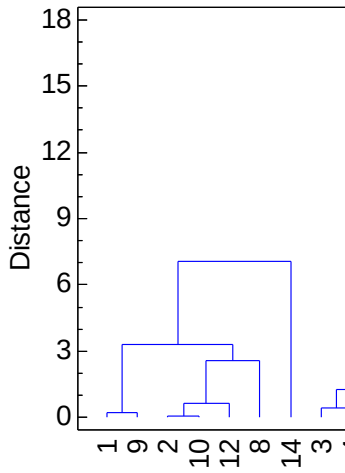

Fig. 20. Dendogram of the cluster analysis (using Ward's method and squared Euclidean distance) for complexes numbered according to Table 2.

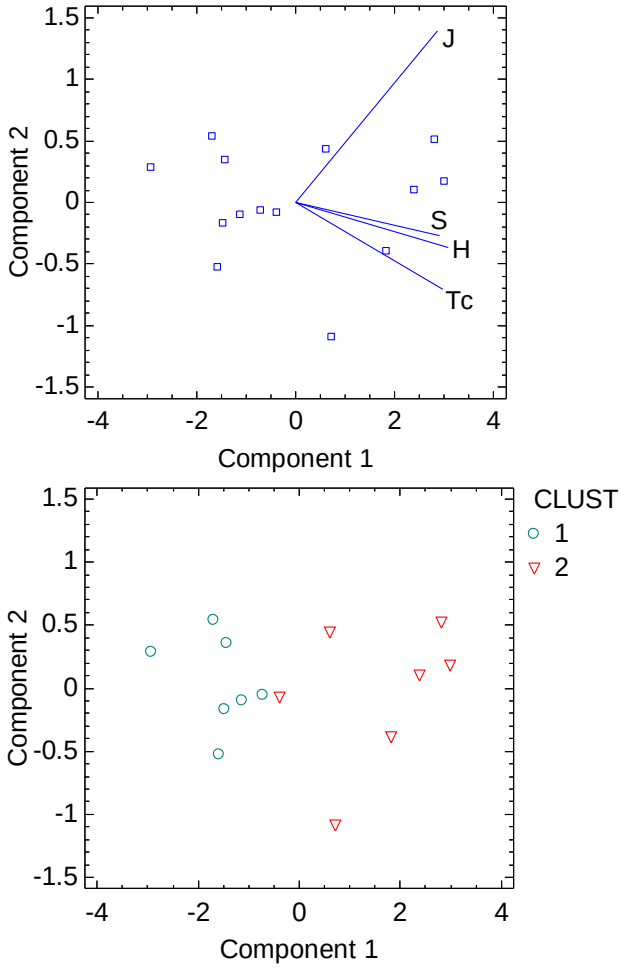

Fig. 21. Results of Principal component analysis. Top – a biplot with a ray diagram, bottom – individual complexes classified by the clusters.

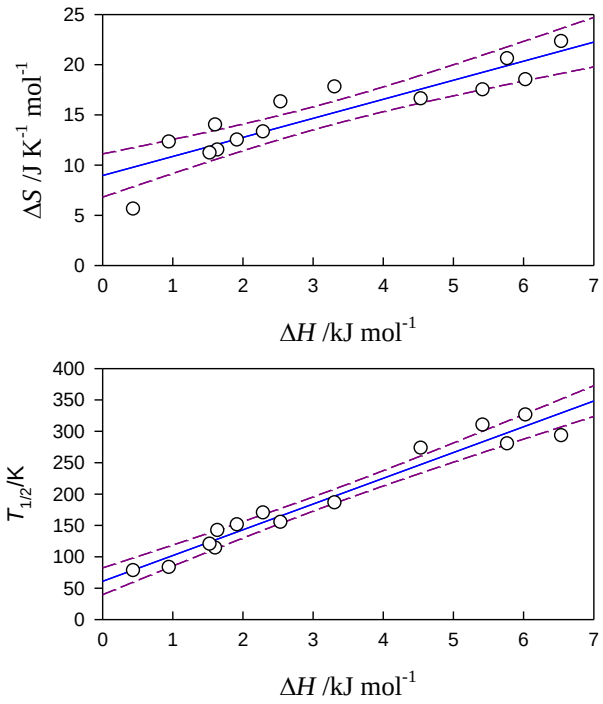

Fig. 22. Linear correlations $T_{1/2}$ *vs* ΔH and ΔS *vs* ΔH. The confidence intervals (95 %) are drawn as dashed curves.

According to Fig. 22 the linear relationship is now confirmed.

The aspects discussed in the present communication are only a part of the huge story, as documented by a number of alterative models and plethora of experiments about the spin crossover phenomenon. Alternative views were comprehensively presented in recent articles (Enachescu *et al.* 2018; Nicolazzi *et al.* 2018; Pavlik *et al.* 2018).

Conclusions

The spin crossover behaviour is based upon a fine tuning of the crystal field strengths balancing the interelectron repulsion. The spin orbit coupling, however, also plays an important role. Ideal thermodynamic behaviour, as described by the regular solution&domain model, is further modified by the interactions in the solid state that are considered as the solid-state cooperativeness. The role of the cooperativeness is analogous to the role of the activity in solution models: it allows using the equation for the ideal system but instead of the mole fraction x_H, an effective mole fraction $J \cdot x_H$ is in the play. The nature of the cooperativeness lies in the electronic (chemical) and nuclear (physical) hardness. Thermo-dynamic data about ΔH and ΔS can be obtained not only from the direct calorimetric measurements but also from an appropriate model of the spin crossover adapted to the magnetic data analysis. These parameters are mutually interrelated through the transition temperature $T_{1/2}$ as proven by the multivariate statistical analysis.

Acknowledgments

Grant agencies of Slovakia are acknowledged for the financial support (projects VEGA 1/0013/18 and APVV 16-0039).

Conflict of Interest

The author declares that he has no conflict of interest.

References

Adler P, Wiehl L, Meibner E, Köhler CP, Spiering H, Gütlich P (1987) The influence of the lattice on the spin transition in solids. Investigations of the high spin ag low spin transition in mixed crystals of $[Fe_xM_{1-x}(2-pic)_3]C1_2 \cdot MeOH$. J. Phys. Chem. Solids 48: 517-525.

Augustín P, Boča R (2015) Magnetostructural relationships for Fe(III) spin crossover complexes. Nova Biotechnol. Chim. 14: 96-103.

Bari RA, Sivardière J (1972) Low-spin-high-spin transitions in transition-metal-ion compounds. Phys. Rev. B5: 4466.

Boča R (2006) Magnetic functions beyond the Spin-Hamiltonian. *In* Mingos DPM (Eds.), Structure and Bonding, 117, Springer, Berlin, Heidenberg, pp. 288.

Boča R (2016) Program MIF&FIT. © University of SS Cyril and Methodius in Trnava, Trnava, unpublished, personal ownership.

Boča R, Boča M, Dlháň K, Falk H, Fuess H, Haase W, Jaroščiak R, Papánková B, Renz F, Vrbová M, Werner R. (2001) Strong cooperativeness in the mononuclear iron(II) derivative exhibiting an abrupt spin transition above 400 K. Inorg. Chem. 40: 3025-3033.

Boča R, Boča M, Ehrenberg H, Fuess H, Linert W, Renz F, Svoboda I (2003) Spin crossover in iron(II) tris(2-(2′-pyridyl)benzimidazole) complex monitored by variable temperature methods: synchrotron powder diffraction, DSC, IR spectra, Mössbauer spectra, and magnetic susceptibility. Chem. Phys. 293: 375-395.

Boča R, Fukuda Y, Gembický M, Herchel R, Jarošiak R, Linert W, Renz F, Yuzurihara J (2000) Spin crossover in mononuclear and binuclear iron(III) complexes with pentadentate Schiff-base ligands. Chem. Phys. Lett. 325: 411-419.

Boča R, Herchel R (2015) Program TERMS. © University

of SS Cyril and Methodius in Trnava, Trnava, unpublished, personal ownership.

Bousseksou A, Constant-Machado H, Varret F (1995) A simple ising-like model for spin conversion including molecular vibrations. J. Phys. I5: 747-760.

Cantin C, Kliava J, Marbeuf A, Mikailitchenko D (1999) Cooperativity in a spin transition ferrous polymer: Interacting domain model, thermodynamic, optical and EPR study. Eur. Phys. J. B12: 525-540.

Enachescu C, Nicolazzi W (2018) Elastic models, lattice dynamics and finite size effects in molecular spin crossover systems. C R Chim. 21: 1179-1195.

Koudriavtsev AB (1999) A modified Bragg and Williams approximation of the two-step spin crossover. Chem. Phys. 241: 109-126.

Krüger C, Augustín P, Dlháň Ľ, Pavlik J, Moncoľ J, Nemec I, Boča R, Renz F (2015) Iron(III) complexes with pentadentate Schiff-base ligands: Influence of crystal packing change and pseudohalido coligand variations on spin crossover. Polyhedron 87: 194-201.

Krüger C, Augustín P, Nemec I, Trávníček Z, Oshio H, Boča R, Renz F (2013) Spin crossover in iron(III) complexes with pentadentate Schiff base ligands and pseudohalido coligands. Eur. J. Inorg. Chem. 2013: 902-915.

Masárová P, Zoufalý P, Moncol J, Nemec I, Pavlik J, Gembický M, Trávníček Z, Boča R, Šalintoš I (2015) Spin crossover and high spin electroneutral mononuclear iron(III) Schiff base complexes involving terminal pseudohalido ligands. New J. Chem. 39: 508-519.

Nakamoto T, Tan Z-C, Sorai M (2001) Heat capacity of the spin crossover complex $[Fe(2\text{-}pic)_3]Cl_2 \cdot MeOH$: a spin crossover phenomenon with weak cooperativity in the solid state. Inorg. Chem. 40: 3805-3809.

Nemec I, Herchel R., Boča R, Trávníček Z, Svoboda I, Fuess H, Linert W (2011) Tuning of spin crossover behaviour in iron(iii) complexes involving pentadentate Schiff bases and pseudohalides. Dalton Trans. 40: 10090-10099.

Nicolazzi W, Bousseksou A (2018) Thermodynamical aspects of the spin crossover phenomenon. C R Chim. 21: 1060-1074.

Pavlik J, Linares J (2018) Microscopic models of spin crossover. C R Chim. 21: 1170-1178.

Person RG (2005) Chemical hardness and density functional theory. J. Chem. Sci. 117: 369-377.

Rao PS, Ganguli P, McGarvey BR (1981) Proton NMR study of the high-spin-low-spin transition in $Fe(phen)_2(NCS)_2$ and $Fe(pic)_3Cl_2$.(EtOH or MeOH). Inorg. Chem. 20: 3682-3688.

Šalintoš I, Boča R, Dlháň Ľ, Gembický M, Kožíšek J, Linares J, Moncoľ J, Nemec I, Perašínová L, Renz F, Svoboda I, Fuess H (2009) Unconventional spin crossover in dinuclear and trinuclear iron(III) complexes with cyanido and metallacyanido bridges. Eur. J. Inorg. Chem. 21: 3141-3154.

Sen KD (1993) Chemical hardness. *In* Structure and bonding, Vol. 80, Springer, Berlin, Heidenberg, 257 p.

Sen KD, Jorgensen CK (1987) Electronegativity. *In* Structure and bonding, Vol. 66, Springer, Berlin, Heidenberg, 198 p.

Slichter CP, Drickamer HG (1972) Pressure-induced electronic changes in compounds of iron. J. Chem. Phys. 56: 2142.

Sorai M, Seki S (1974) Phonon coupled cooperative low-spin $^1A1$high-spin $^5T_2$ transition in $[Fe(phen)_2(NCS)_2]$ and $[Fe(phen)_2(NCSe)_2]$ crystals. J. Phys. Chem. Solids 35: 555-570.

Spiering H, Meissner E, Köppen H, Müller EW, Gütlich P (1982) The effect of the lattice expansion on high spin ⇌ low spin transitions. Chem. Phys. 68: 65-71.

Statgraphics Centurion XV. © Statpoint Inc., 2006.

Wajnflasz J (1970) Etude de la transition „Low Spin"-„High Spin" dans les complexes octaédriques d'ion de transition. J. Phys. Stat. Sol. 40: 537-545.

Wass JA (1999) Mathematica 4.0. Science 286, p. 2291.

Zimmermann R, König E (1977) A model for high-spin/low spin transitions in solids including the effect of lattice vibrations. J. Phys. Chem. Solids 38: 779-788.